

Received May 15, 2016, accepted June 7, 2016, date of publication June 20, 2016, date of current version July 7, 2016.

Digital Object Identifier 10.1109/ACCESS.2016.2580594

Spectral Matrix Decomposition-Based Motion Artifacts Removal in Multi-Channel PPG Sensor Signals

JIPING XIONG¹, (Member, IEEE), LISANG CAI¹, (Student Member, IEEE),
DINGDE JIANG², (Member, IEEE), HOUBIND SONG³, (Senior Member, IEEE),
AND XIAOWEI HE¹, (Member, IEEE)

¹College of Mathematics, Physics and Information Engineering, Zhejiang Normal University, Jinhua, Zhejiang 321004, China

²College of Information Science and Engineering, Northeastern University, Shenyang, Liaoning 110819, China

³Department of Electrical and Computer Engineering, West Virginia University, Montgomery, WV 25136-2436, USA

Corresponding authors: J. Xiong (xjp@zjnu.cn) and D. Jiang (jiangdd@mail.neu.edu.cn)

This work was supported in part by the National Natural Science Foundation of China under Grant 61572023, Grant 61571104, and Grant 61572231, in part by the Zhejiang Provincial Natural Science Foundation of China under Grant LY14F010008, in part by the General Project of Scientific Research of the Education through the Department of Liaoning Province under Grant L20150174, in part by the Fundamental Research Funds for the Central Universities under Grant N150402003, and in part by the State Scholarship Fund under Grant 201208210013.

ABSTRACT The intelligent wearable heart rate measurement requirement has attracted more and more attention, and the related applications of Internet of Things are emerging. However, under intensive physical exercises, motion artifacts are strong interference sources for wrist-type photoplethysmography (PPG) sensor signals, thus significantly affecting the accurate estimation of heart rate and other physiological parameters. Currently, how to effectively remove the motion artifacts from PPG sensor signals is becoming an active and challenging research realm. In this paper, we propose a multi-channel spectral matrix decomposition (MC-SMD) model to accurately estimate heart rate in the presence of intensive physical activities. Motivated by the observation that the PPG signal spectrum and the acceleration spectrum have almost the same spectral peak positions in the frequency domain, we first model the removal of motion artifacts as a spectral matrix decomposition optimization problem. After removing motion artifacts, we propose a new spectral peak tracking method for estimating heart rate. Experimental results on the well-known PPG data sets recorded from 12 subjects during intensive movements demonstrate that MC-SMD can efficiently remove the motion artifacts and retrieve an accurate heart rate using multi-channel PPG sensor signals.

INDEX TERMS Accelerated proximal gradient (APG) method, compressive sensing, heart rate measurement, photoplethysmography (PPG).

I. INTRODUCTION

A. BACKGROUND AND MOTIVATION

With the rapid development of electronics technology miniaturization [1], the monitoring of human health is gaining more and more attention. One public health report in 2010 showed that almost 1 in every 4 deaths every year in the United States is due to heart disease [2]. Hence, heart rate monitoring is always regarded as having great importance among all monitored vital signs. Recently, photoplethysmography (PPG) [3], [4] has become an efficient and popular estimation method for heart rate estimation. Compared with an electrocardiogram (ECG), which is obtained from

the chest without body movement, PPG sensor signals are obtained via a non-invasive method [5], [6]. More importantly, PPG sensors are simple, low-cost, easy-to-use, and do not require specific techniques to be attached to skin.

Despite the attractive attributes of PPG, a major disadvantage of PPG is that it is sensitive and vulnerable to human physical motion. Therefore, to decode heart health status more reliably, the motion artifacts introduced by physical motion must be extracted and rejected from the original noisy PPG sensor signals. However, the motion artifacts component can mostly mask the heart rate information during intensive physical exercise; thus, removal of the

motion artifacts in raw PPG sensor signals is a challenging task [7].

B. STATE-OF-THE-ART

To date, researchers have presented numerous signal processing approaches to removing motion artifacts in PPG, such as wavelet-based method [8]–[10], empirical mode decomposition (EMD) [11], [12], Kalman filtering [13], time-frequency analysis [14], non-line methods [15], spectrum subtraction [16], independent component analysis (ICA) [17], and adaptive noise cancellation (ANC) [18], [19], to name a few. However, the above methods were mainly proposed for clinical scenarios when subjects performed some small motions.

For strong motion artifacts, Zhang *et al.* [20], [21] proposed a TROIKA framework, which consists of signal decomposition, sparse signal reconstruction and spectral peak tracking with verification. The signal decomposition stage is used to partially remove motion artifacts. Then, a high resolution spectrum of the PPG signal can be calculated using sparse signal reconstruction. The spectral peak tracking with the verification stage facilitates the finding of spectral peaks corresponding to heart rate. Zhilin Zhang proposed another approach, i.e., JOSS [22]. This approach exploits the common spectral structures between the PPG signal and the accelerometer signals. Moreover, it includes the multiple measurement vector (MMV) model, spectrum subtraction and spectral peak tracking. Compared with the TROIKA framework, the JOSS method further improves the denoising performance.

Meanwhile, Zhu *et al.* [23] proposed the MICROST framework. It was designed as a mixed algorithm that consists of acceleration classification (AC), first-frame processing and heuristic tracking. Sun and Zhang [24] proposed the SPECTRAP method. This method first calculates the spectra of the PPG signal and the acceleration signal and then removes the motion artifacts' spectral components using a new spectrum subtraction algorithm. In [25], a novel algorithm that consists of motion artifacts cancellation and spectral analysis was proposed. The motion artifacts cancellation step cleanses the contaminated PPG sensor signals, utilizing the acceleration data, while the spectral analysis step estimates a higher spectrum of the signal and chooses the spectral peaks corresponding to heart rate. However, the main drawbacks of these methods are that the denoising process does not make use of the sparsity of the PPG sensor signals and the strong relativity between the PPG sensor signals and the acceleration signals.

C. CONTRIBUTIONS AND PAPER ORGANIZATION

The study aims to improve heart rate estimation performance while solving the aforementioned drawbacks. A novel denoising algorithm for heart rate estimation is proposed, which is based on Multi-Channel Spectral Matrix Decomposition, denoted by MC-SMD. Firstly, we construct a spectral matrix using multi-channel PPG sensor signals and acceleration signals during the same time period. Next, the spectral

matrix is divided into a motion artifacts matrix and real PPG sensor signals matrix. Finally, we use the spectral peak tracking methods to estimate heart rate.

The remainder of this paper is organized as follows. Section II describes our MC-SMD model in detail. Section III presents the framework of heart rate measurement. Section IV presents the experimental results. The conclusion is given in the last section.

II. PROPOSED FRAMEWORK

A. MULTI-CHANNEL SPECTRAL MATRIX DECOMPOSITION MODEL

The MMV model [22] is an extension of the single measurement vector (SMV) model [20], [21], which can estimate a solution jointly from multiple measurement vectors. When estimating the power spectra of multi-channel signals, we can model the procedure as follows

$$Y = \Phi X + V. \quad (1)$$

where $Y \in R^{M \times H}$ is the matrix consisting of H measurement vectors, $\Phi_{m,n} = e^{j\frac{2\pi}{N}mn} \in C^{M \times N}$ ($M < N$) is the redundant discrete Fourier transform (DFT) basis, $X \in C^{N \times H}$ is the desired solution matrix (i.e., the sparse matrix), and $V \in R^{M \times H}$ represents measurement noise or model errors. We adopt the Regularized M-FOCUSS algorithm [26] to solve Eq. (1), because here the matrix Φ is highly coherent.

Motivated by the SMV model [20], [21] and the MMV model [22], we first divide the spectral matrix into the motion artifacts matrix and real PPG sensor signals matrix. This can be expressed as follows

$$X = P + Q. \quad (2)$$

where X is the sparse matrix as before, P is the motion artifacts spectral matrix, and Q is the real PPG sensor signals spectral matrix.

Because the periodicity of the cleaned PPG sensor signals corresponds to the cardiac rhythm [27], the cleaned PPG sensor signals have sparsity in the frequency domain. The PPG spectrum and the acceleration spectrum almost have the same spectral peak positions in the frequency domain because of the strong relativity between PPG sensor signals and acceleration signals. Hereby, combined with the compressive sensing theory, the MC-SMD model can be expressed as follows

$$\begin{aligned} \min_{P,Q} \quad & \frac{1}{2} \|Y - \Phi(P + Q)\|_F^2 + \lambda_1 \|P\|_{1,2} + \lambda_2 \|Q\|_{1,1}; \\ \text{s.t. : } \quad & Y = \Phi(P + Q). \end{aligned} \quad (3)$$

where $\|P\|_{1,2} = \sum_{i=1}^N \left(\sum_{j=1}^R p_{i,j}^2 \right)^{\frac{1}{2}}$, $\|Q\|_{1,1} = \sum_{i=1}^N \sum_{j=1}^R |q_{i,j}|$ are used to constrain the row sparse of motion artifacts spectral matrix and whole sparse of real PPG sensor signals spectral matrix, respectively. $p_{i,j}$ denotes the (i, j) th entry of P , while $q_{i,j}$ denotes the (i, j) th entry of Q . λ_1, λ_2 are weights used to trade-off the importance of P, Q items.

Note that the measurement matrix Y contains multi-channel PPG sensor signals in the MC-SMD model. In the experiments, only two channel PPG sensor signals were used. Thus, the first and second column of Y denote two PPG sensor signals (namely, PPG1, PPG2, respectively). The other three columns denote the acceleration signals of three directions.

B. MULTI-CHANNEL SPECTRAL MATRIX DECOMPOSITION MODEL USING ACCELERATED PROXIMAL GRADIENT METHOD

We find that the objective function (3) is composed of two parts: the differential experience cost function $L(P, Q)$ and the convex non-smooth regularization part $G(P, Q)$, i.e.,

$$L(P, Q) = \frac{1}{2} \|Y - \Phi(P + Q)\|_F^2. \quad (4)$$

$$G(P, Q) = \lambda_1 \|P\|_{1,2} + \lambda_2 \|Q\|_{1,1}. \quad (5)$$

It is well known that this kind of objective function has been studied in [28]–[30]. In this paper, we adopt the Accelerated Proximal Gradient (APG) method to solve Eq. (3). Compared with the traditional sub-gradient-based methods, APG has a better convergence rate. It can obtain the global optimal solution with a quadratic convergence rate. Namely, APG can acquire the optimal solution with $O(1/m^2)$ residual after m iterations.

Thus, we utilize the composite gradient mapping [28] method to rewrite Eq. (3) in the following form:

$$\begin{aligned} F(P, Q; \Theta, \Psi) &= L(\Theta, \Psi) + \langle \nabla_P L(\Theta, \Psi), P - \Theta \rangle \\ &\quad + \frac{\eta}{2} \|P - \Theta\|_F^2 + \langle \nabla_Q L(\Theta, \Psi), Q - \Psi \rangle \\ &\quad + \frac{\eta}{2} \|Q - \Psi\|_F^2 + G(P, Q). \end{aligned} \quad (6)$$

where $F(P, Q; \Theta, \Psi)$ consists of the regularization term $G(P, Q)$ and the first order Taylor expansion $L(P, Q)$ at point (Θ, Ψ) . The square of the Euclidean distance between (P, Q) and (Θ, Ψ) denotes the remainder term of the Taylor expansion. $\nabla_P L(\Theta, \Psi)$ and $\nabla_Q L(\Theta, \Psi)$ denote the partial derivatives of $L(P, Q)$ about P and Q , respectively. η is the parameter for controlling step length.

In the m -th iteration of APG, the linear combination of (P^m, Q^m) and (P^{m+1}, Q^{m+1}) can form $(\Theta^{m+1}, \Psi^{m+1})$; thus, $(\Theta^{m+1}, \Psi^{m+1})$ stores the historical information of (P, Q) in the previous iteration process. Generally, the process is called the aggregation step. The updated results of $(\Theta^{m+1}, \Psi^{m+1})$ can be expressed as follows

$$\Theta^{m+1} = P^m + \alpha_m \left(\frac{1 - \alpha_{m-1}}{\alpha_m} \right) (P^m - P^{m-1}). \quad (7)$$

$$\Psi^{m+1} = Q^m + \alpha_m \left(\frac{1 - \alpha_{m-1}}{\alpha_{m-1}} \right) (Q^m - Q^{m-1}). \quad (8)$$

where $\alpha_m = 1$ when $m = 0$ and $\alpha_m = \frac{2}{m+3}$ when $m > 1$.

Once (Θ^m, Ψ^m) is given, we can obtain the solution of the m -th iteration by solving the following optimization problem.

$$(P^m, Q^m) = \arg \min_{P, Q} F(P, Q; \Theta^m, \Psi^m). \quad (9)$$

To better describe the solving process, we first give two conclusions, defined as Eq. (10) and Eq. (11) [31], [32].

$$X^* = \arg \min \varepsilon \|X\|_{1,1} + \frac{1}{2} \|X - R\|_F^2 = S_\varepsilon(R). \quad (10)$$

$$X^* = \arg \min \varepsilon \|X\|_{1,2} + \frac{1}{2} \|X - R\|_F^2 = W_\varepsilon(R). \quad (11)$$

where $S_\varepsilon(R_{i,j})$ denotes a soft threshold operation, which can be defined as Eq. (12). The computation rules of $W_\varepsilon(R)$ can be expressed as Eq. (13).

$$S_\varepsilon(R_{i,j}) = \operatorname{sgn}(R_{i,j}) \max(0, |R_{i,j}| - \varepsilon). \quad (12)$$

$$W_\varepsilon(R)_{i,:} = \begin{cases} \left(1 - \frac{\varepsilon}{\|r_i\|}\right) r_i & \varepsilon < \|r_i\| \\ \vec{0} & \text{otherwise.} \end{cases} \quad (13)$$

where r_i denotes the i -th row of R .

Then, the optimization problem of Eq. (9) can be decomposed into two sub-problems for P and Q , respectively, i.e.,

$$\begin{aligned} P^m &= \arg \min_P \frac{\lambda_1}{\eta} \|P\|_{1,2} \\ &\quad + \frac{1}{2} \|P - \Theta^m + 1/\eta \nabla_P L(\Theta^m, \Psi^m)\|_F^2. \\ &\Rightarrow W_{\frac{\lambda_1}{\eta}}(\Theta^m - 1/\eta \nabla_P L(\Theta^m, \Psi^m)). \end{aligned} \quad (14)$$

$$\begin{aligned} Q^m &= \arg \min_Q \frac{\lambda_2}{\eta} \|Q\|_{1,1} \\ &\quad + \frac{1}{2} \|Q - \Psi^m + 1/\eta \nabla_Q L(\Theta^m, \Psi^m)\|_F^2. \\ &\Rightarrow S_{\frac{\lambda_2}{\eta}}(\Psi^m - 1/\eta \nabla_Q L(\Theta^m, \Psi^m)). \end{aligned} \quad (15)$$

In general, the process of the whole optimization algorithm can be summarized as in algorithm 1.

Algorithm 1 APG Algorithm

Input: $Y, \Phi, P^0, Q^0, \eta, \lambda_1, \lambda_2$

Output: P, Q .

Initialization: $m = 1, P^0 = 0, Q^0 = 0, \Theta^1 = 0, \Psi^1 = 0$.

while not converged **do**

Compute $\nabla_P L(\Theta^m, \Psi^m)$ and $\nabla_Q L(\Theta^m, \Psi^m)$.

Compute P^m and Q^m using Eq. (14), (15).

$$\alpha_m = \frac{2}{m+3}.$$

$$\Theta^{m+1} = P^m + \alpha_m \left(\frac{1 - \alpha_{m-1}}{\alpha_m} \right) (P^m - P^{m-1}).$$

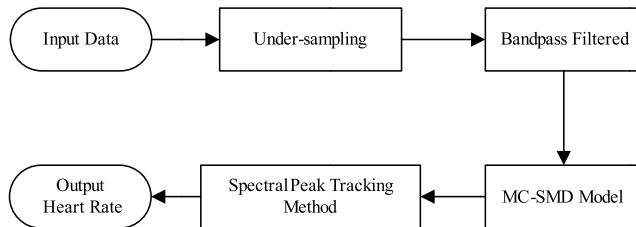
$$\Psi^{m+1} = Q^m + \alpha_m \left(\frac{1 - \alpha_{m-1}}{\alpha_{m-1}} \right) (Q^m - Q^{m-1}).$$

$$m = m + 1.$$

End while

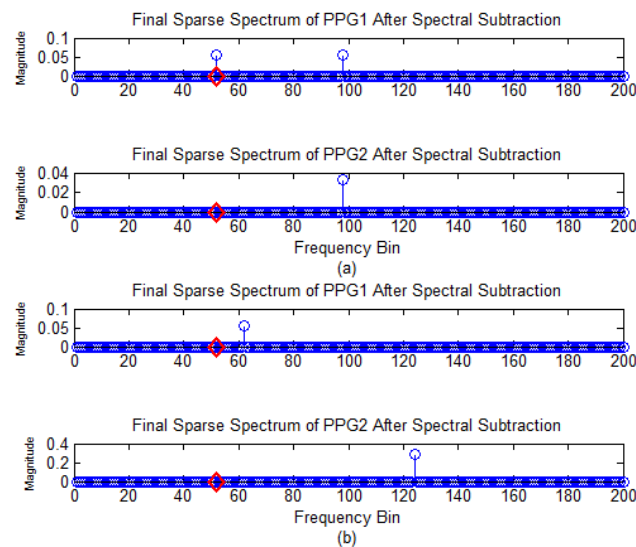
III. HEART RATE ESTIMATION

Fig. 1 is the flowchart of our heart rate estimation. The spectral peak tracking method can deal with some extreme conditions and retrieve the frequency locations of a heart rate precisely.

**FIGURE 1.** Flowchart of heart rate estimation.

A. SPECTRAL PEAK TRACKING

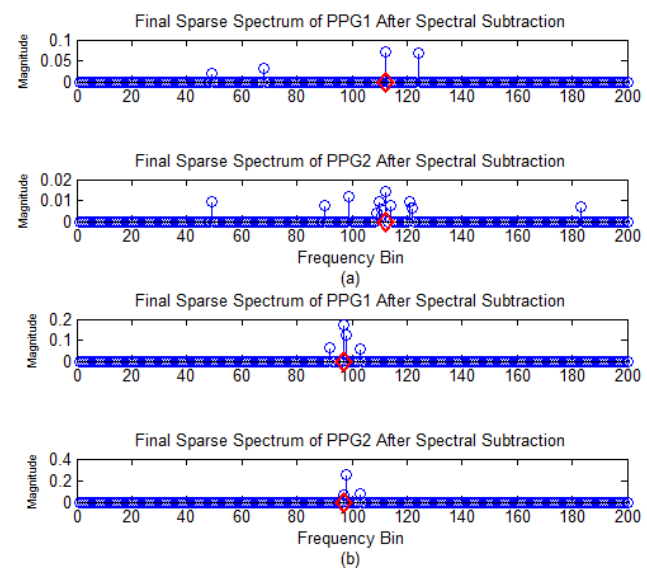
We can obtain the real PPG spectra and motion artifacts spectra by solving the MC-SMD model. In this section, we mainly utilize the real PPG spectra to identify the spectral peaks corresponding to heart rate. Because the real PPG spectra may have some extreme situations, to ensure the accuracy of heart rate estimation, we propose an effective spectral peak tracking method that can handle these extreme situations containing the no-peak condition (shown in Fig. 2) and the multi-peak condition (shown in Fig. 3).

**FIGURE 2.** No-peak condition. Red diamond tag is the true heartbeat frequency (estimated from the ECG signal). (a) There are heart rate peaks in PPG1 but no heart rate spectral peaks in PPG2. (b) There are no heart rate peaks both in PPG1 and PPG2.

Our spectral peak tracking method mainly consists of three stages: initialization, peak selection and peak detection (given two-channel PPG spectra and three-channel acceleration spectra).

1) Initialization: The initialization stage is done in a manner similar to the process proposed by Zhang [22]. In this stage, wearers are required to reduce hand motions as much as possible for several seconds. Heart rate is estimated by choosing the highest spectral peak in the PPG1 spectrum.

We use the kurtosis of the PPG1 spectrum from 0.8 Hz to 2.5 Hz to classify whether hand motions are reduced sufficiently. If the kurtosis is larger than 10, the current time

**FIGURE 3.** Multi-peak condition. Red diamond tag is the true heartbeat frequency (estimated from the ECG signal). (a) There are multiple motion artifact peaks near heart rate peaks in PPG2. (b) There are multiple motion artifact peaks near heart rate peaks both in PPG1 and PPG2.

window is determined to be in the initialization stage and we select the highest spectral peak in the PPG1 spectrum from 0.8 Hz to 2.5 Hz; in the next time window, the approach enters the next stage. Otherwise, the current time window is not in the initialization stage and no heart rate estimate is output; in the next time window, we need to again perform this process to check whether it is in the initialization stage.

TABLE 1. The meaning of variables.

Variables	The meaning of variables
$pc1, pc2$	The spectral peak numbers of PPG1, PPG2 in the search range, respectively.
$mpLoc1, mpLoc2$	The highest peak of PPG1, PPG2 respectively in Δ_1 .
$cLoc1, cLoc2$	The peak of PPG1, PPG2 closest to $prevLoc1$ in Δ_1 , respectively.
$cLoc$	The one closest to $prevLoc1$ between $cLoc1$ and $cLoc2$.
$Trap_count$	The counter is used to calculate the number of abnormal estimated heart rates.
$ID1, ID2$	The highest peak of PPG1, PPG2 respectively in Δ_2 .
Loc	The peak of PPG2 closest to $prevLoc1$ in Δ_2 .
ID	The one closest to $prevLoc1$ between $ID1$ and $ID2$.

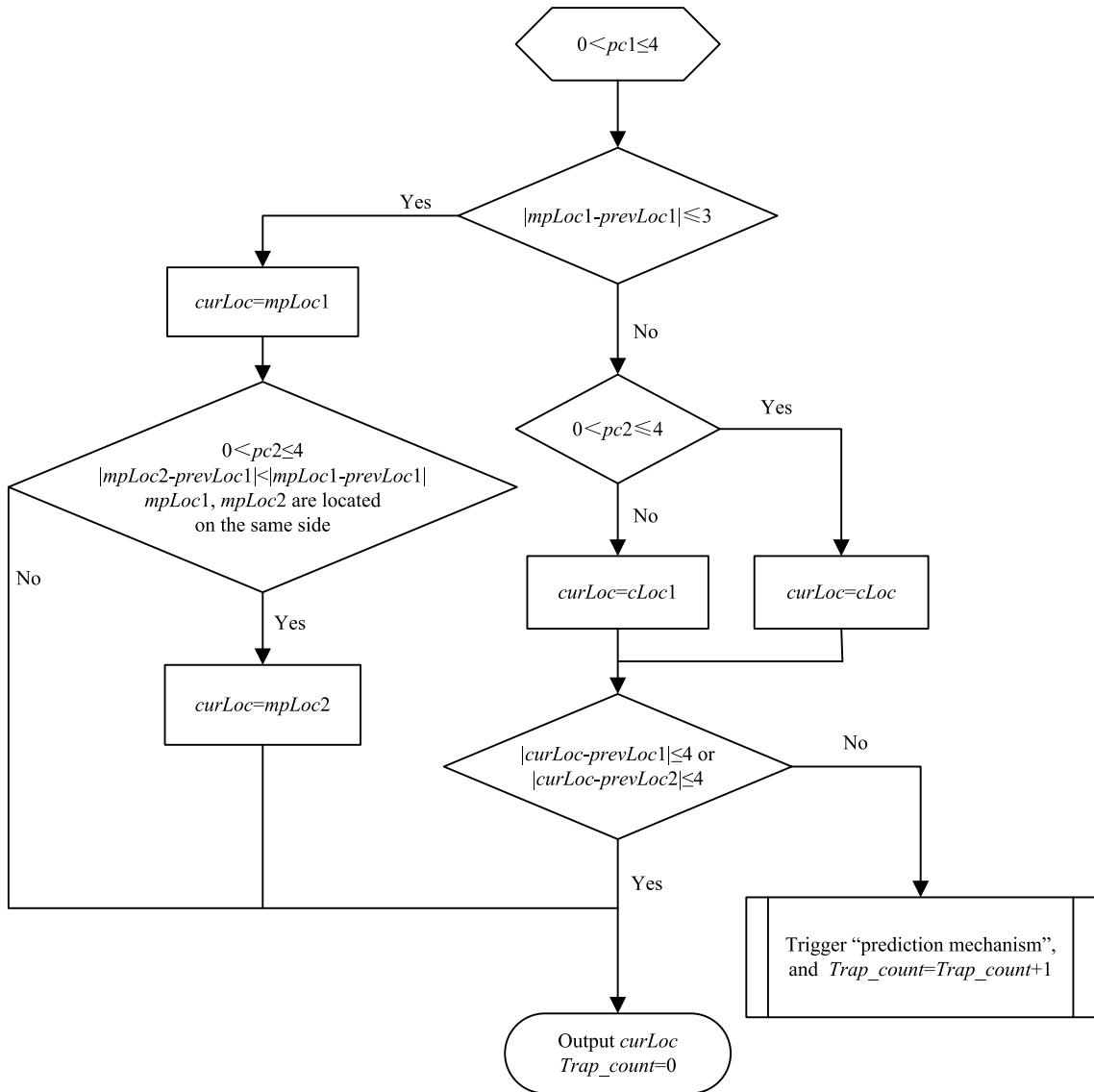


FIGURE 4. Flowchart of case 1.

2) Peak Selection: In this stage, the goal is to choose peaks in the PPG1 and PPG2 spectra with the knowledge of estimated heart rate values from previous time windows.

We need to determine the spectral peak location of the heart rate in the current time window for three cases. To better understand the following procedure, some variables are shown in Table 1.

First, a search range denoted as Δ_1 is set. This search range is centered at the location of the previously estimated spectral peak. Then, denoted as $prevLoc1$, the frequency bin corresponding to the previously estimated heart rate, i.e., $\Delta_1 = [prevLoc1 - R_1, prevLoc1 + R_1]$, where $R_1 = 7$ is a positive integer, is set.

Case 1: In the search range Δ_1 , $0 < pc1 \leq 4$; the flowchart is given in Fig. 4.

(a) If $|mpLoc1 - prevLoc1| \leq 3$, we select the one (namely, $mpLoc1$) with the highest value; thus, $mpLoc1$ is the frequency location index of the heart rate (namely, $curLoc$) in the current time window.

(b) If (a) condition is established and $0 < pc2 \leq 4$, $|mpLoc2 - prevLoc1| < |mpLoc1 - prevLoc1|$, $mpLoc1$ and $mpLoc2$ are located on the same side; then, we choose $mpLoc2$ instead of $mpLoc1$.

(c) If (a) condition is not established and $0 < pc2 \leq 4$, then we select the one (namely, $cLoc$) closest to $prevLoc1$ between $cLoc1$ and $cLoc2$.

(d) If (a) and (c) conditions are not established, we can select the one (namely, $cLoc1$) closest to $prevLoc1$ in the PPG1 spectrum.

To ensure the rationalization of the selected $curLoc$, we propose a validation mechanism. Namely, if

$|curLoc - prevLoc1| \leq 4$ or $|curLoc - prevLoc2| \leq 4$ ($prevLoc2$ denotes the frequency bin corresponding to the estimated heart rate in the penultimate time window), then the validation mechanism output $curLoc$ and $Trap_count = 0$. Otherwise, we need to trigger a prediction mechanism and $Trap_count = Trap_count + 1$.

The prediction mechanism is used to solve problem where we cannot find the spectral peak locations corresponding to the heart rate in the PPG1 and PPG2 spectra. The mechanism can be expressed as follows:

$$curLoc = \begin{cases} prevLoc1 + 2 & \text{if } h > 0; \\ prevLoc1 - 2 & \text{if } h < 0; \\ prevLoc1 & \text{if } h = 0. \end{cases} \quad (16)$$

where $h = predictLoc1 - predictLoc2$, $predictLoc1$ is the predicted spectral peak location in the current time window, and $predictLoc2$ is the predicted spectral peak location in the previous time window. Then, we utilize the Smoother algorithm [33] to acquire $predictLoc1$ and $predictLoc2$. The algorithm is performed using the spectral peak positions of the 10 closest previously estimated heart rate values; the smoother parameter is set to 20.

We may face a situation in which two peaks have equal distance to $prevLoc1$ (one has lower frequency and the other has higher frequency) when we select the peak closest to $prevLoc1$. To deal with this situation, we put forward an effective approach. If $prevLoc1 - prevLoc2 > 0$, then select the higher frequency. If $prevLoc1 - prevLoc2 \leq 0$, then select the lower frequency.

Case 2: When $pc1 \geq 5$, denoted as multi-peak. The flowchart is shown in Fig. 5. We set another search range $\Delta_2 = [prevLoc1 - R_2, prevLoc1 + R_2]$, where $R_2 = 5$.

(a) If $0 < pc2 \leq 4$ and $|ID2 - prevLoc1| \leq 3$, then we select the one (namely, $ID2$) with the highest value and $Trap_count = 0$.

(b) If (a) condition is not established and $0 < pc2 \leq 4$, $|Loc - prevLoc1| \leq 2$, then we select the one (namely, Loc) closest to $prevLoc1$ in the PPG2 spectrum and $Trap_count = 0$.

(c) If (a) and (b) conditions are not established and the highest spectral peak locations are the same (namely, $ID1 = ID2$) in the PPG1 and PPG2 spectra, $|ID1 - prevLoc1| \leq 3$, then we select $ID1$ as $curLoc$ and $Trap_count = 0$.

(d) If (a), (b) and (c) conditions are not established and $|ID - prevLoc1| \leq 2$, then we select the one (namely, ID) closest to $prevLoc1$ between $ID1$ and $ID2$ and $Trap_count = 0$. Otherwise, we need to trigger the prediction mechanism and $Trap_count = Trap_count + 1$.

Case 3: When $pc1 = 0$, denoted as no-peak. The flowchart is shown in Fig. 6. Here, we still use the search range $\Delta_2 = [prevLoc1 - R_2, prevLoc1 + R_2]$.

(a) If $pc2 > 0$ and $|ID2 - prevLoc1| \leq 3$, then we choose the one (namely, $ID2$) with the highest value and $Trap_count = 0$.

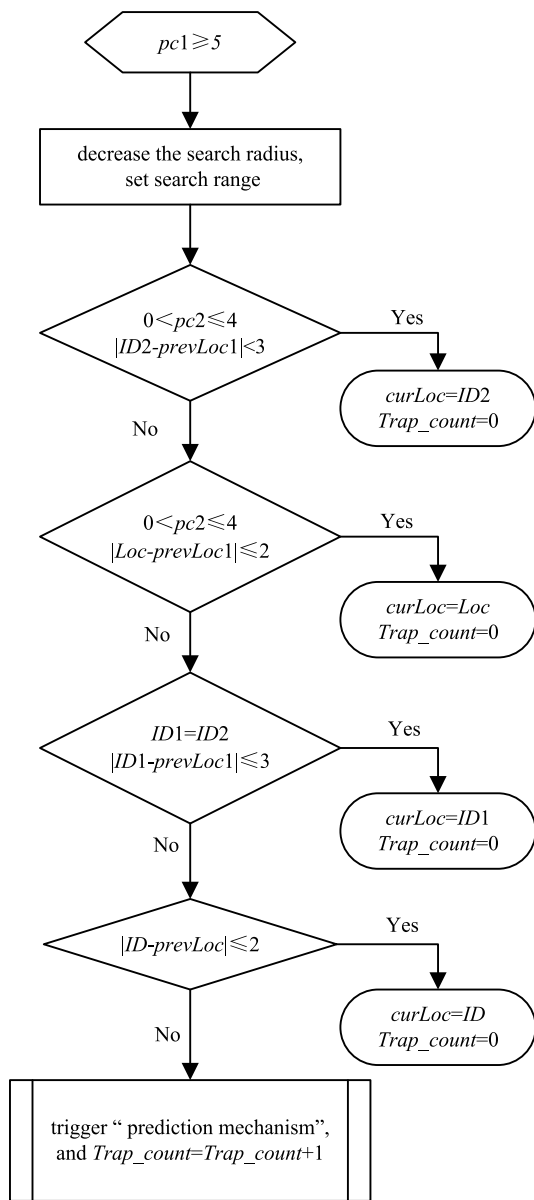


FIGURE 5. Flowchart of case 2.

(b) If (a) condition is not established and $0 < pc2 \leq 4$, $|Loc - prevLoc1| \leq 4$, then we choose the one (namely, Loc) closest to $prevLoc1$ in the PPG2 spectrum and $Trap_count = 0$. If not, we need to trigger the prediction mechanism and $Trap_count = Trap_count + 1$.

3) Peak Detection: This stage can prevent the spectral peaks corresponding to the heart rate from being lost effectively. When the counter $Trap_count \geq 3$, it indicates that the target spectral peak may be lost. Thus, a peak discovery procedure is triggered.

First, a larger search range than before is set. The search range is $\Delta_3 = [centerLoc - R_3, centerLoc + R_3]$, where $centerLoc$ denotes the estimated spectral peak location when $Trap_count = 0$ (in the next time window, $Trap_count = 1$) and $R_3 = 10$.

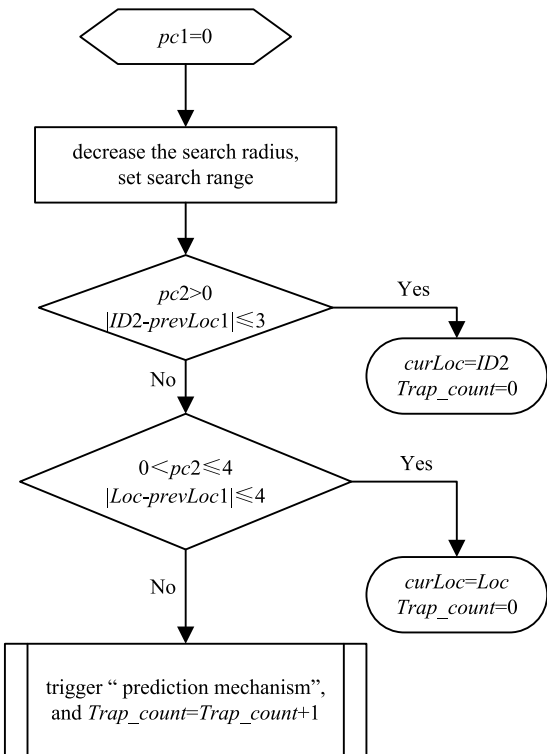
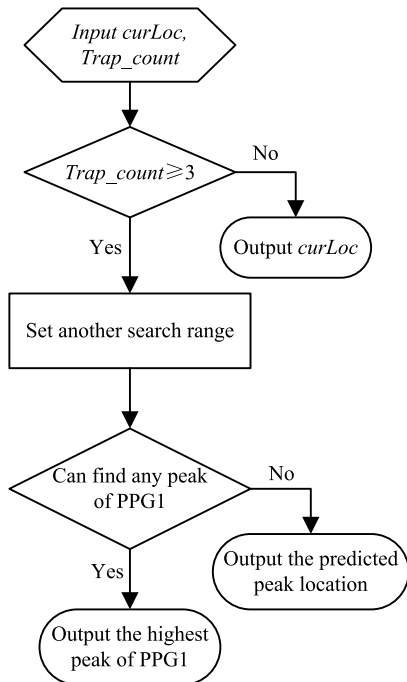
**FIGURE 6.** Flowchart of case 3.**FIGURE 7.** Flowchart of the peak discovery procedure.

Fig. 7 shows the flowchart of peak discovery. We first judge whether the spectral peaks exist in the PPG1 spectrum. If we find any, then the one with highest value is selected. If not, the spectral peak is predicted by performing the Smoother

algorithm in the current time window. The algorithm is performed for the spectral peak positions of the 15 closest previously estimated heart rate values; the smoother parameter is set to 20.

IV. EXPERIMENTAL RESULTS

A. DATA DESCRIPTION

We validated our method using a published database of IEEE Signal Process Cup 2015 [34]. Data was collected from 12 healthy male subjects with yellow skin and ages ranging from 18 to 35. Each dataset consists of two-channel PPG sensor signals, three-axis simultaneous acceleration signals, and a one-channel ECG signal recorded by using pulse oximeters (Green LED: 515 nm), an accelerometer on the wrist and wet ECG sensors on the chest, respectively. Both the pulse oximeters and the accelerometer were embedded in a comfortable wristband, and two pulse oximeters, placed 2-cm apart (from center to center), were used. Then, the ground-truth of the heart rate was calculated from the ECG signal, which was used to evaluate the algorithms' performance. Note that we did not use any ECG heart rate estimation algorithms to avoid estimation errors. All signals were wirelessly transmitted to a nearby computer or mobile phone.

During the recording of the 12 datasets, the subjects walked or ran on a treadmill at the following speeds, in order: 1-2 km/hour for 0.5 minute, 6-8 km/hour for 1 minute, 12-15 km/hour for 1 minute, 6-8 km/hour for 1 minute, 12-15 km/hour for 1 minute, and 1-2 km/hour for 0.5 minute. In this process, the subjects were asked to purposely do some motions, such as pulling clothes, wiping sweat on forehead, pushing buttons on the treadmill, and freely swinging hands.

Note that all signals were sampled at 125 Hz initially. Then, the multi-channel PPG sensor signals and the simultaneous acceleration signals were down-sampled to 25 Hz to guarantee high computational efficiency.

B. PARAMETER SETTINGS

Heart rate estimation was done for each 8-second window (200 samples), with a shift of 2 seconds (50 samples). Before performing MC-SMD, all raw signals were processed using a 2nd order Butterworth filter, with a low cut-off frequency and a high cut-off frequency of 0.4 Hz and 4 Hz, respectively.

Meanwhile, the relevant parameters in the experiments were adjusted as follows: the weighting parameters in Eq. (3), to $\lambda_1 = 0.01$, $\lambda_2 = 1.1$; the spectrum grid parameter in DFT, $N = 1024$. For the spectral peak tracking, the relevant parameters have been explained in section III; thus, they will not be repeated here.

C. PERFORMANCE MEASUREMENT

In each time window, the number of cardiac cycles H and the duration D (in seconds) were counted; then, the heart rate was calculated as $60H/D$ (in BPM).

TABLE 2. The average absolute errors (error1) for 12 datasets (unit: BPM).

	Set1	Set2	Set3	Set4	Set5	Set6	Set7	Set8	Set9	Set10	Set11	Set12	Average
TROIKA [20]	2.87	2.75	1.91	2.25	1.69	3.16	1.72	1.83	1.58	4.00	1.96	3.33	2.42
JOSS [21]	1.33	1.75	1.47	1.48	0.69	1.32	0.71	0.56	0.49	3.81	0.78	1.04	1.28
MICROST [22]	2.93	3.06	2.03	2.29	2.64	2.58	1.97	1.77	1.87	3.81	1.91	4.07	2.58
SPECTRAP [23]	1.18	2.42	0.86	1.38	0.92	1.37	1.53	0.64	0.60	3.65	0.92	1.25	1.50
Literature [24]	1.72	1.33	0.90	1.28	0.93	1.41	0.61	0.88	0.59	3.78	0.85	0.71	1.25
MC-SMD	1.16	1.07	0.80	1.13	0.98	1.29	0.88	0.81	0.55	3.18	0.79	0.72	1.11

TABLE 3. The average absolute errors percentages (error2) for 12 datasets.

	Set1	Set2	Set3	Set4	Set5	Set6	Set7	Set8	Set9	Set10	Set11	Set12	Average
TROIKA [20]	2.18%	2.37%	1.50%	2.00%	1.22%	2.51%	1.27%	1.47%	1.28%	2.49%	1.29%	2.30%	1.82%
JOSS [21]	1.19%	1.66%	1.27%	1.41%	0.51%	1.09%	0.54%	0.47%	0.41%	2.43%	0.51%	0.81%	1.01%
MICROST [22]	2.55%	2.94%	1.60%	1.89%	1.80%	2.03%	1.49%	1.50%	1.64%	2.39%	1.31%	2.76%	1.99%
SPECTRAP [23]	1.04%	2.33%	0.66%	1.31%	0.74%	1.14%	1.36%	0.55%	0.52%	2.27%	0.65%	1.02%	1.12%
Literature [24]	1.5%	1.3%	0.75%	1.2%	0.69%	1.2%	0.5%	0.8%	0.5%	2.4%	0.6%	0.5%	0.99%
MC-SMD	0.91%	0.87%	0.62%	0.84%	0.68%	0.96%	0.65%	0.64%	0.43%	1.95%	0.51%	0.53%	0.80%

To evaluate the performance of MC-SMD, four measuring objects were used in the paper. The average absolute error (Error1) and the average absolute error percentage (Error2) were computed as

$$\text{Error1} = \frac{1}{W} \sum_{i=1}^W |\text{BPM}_{\text{est}}(i) - \text{BPM}_{\text{true}}(i)|. \quad (17)$$

$$\text{Error2} = \frac{1}{W} \sum_{i=1}^W \frac{|\text{BPM}_{\text{est}}(i) - \text{BPM}_{\text{true}}(i)|}{\text{BPM}_{\text{true}}(i)}. \quad (18)$$

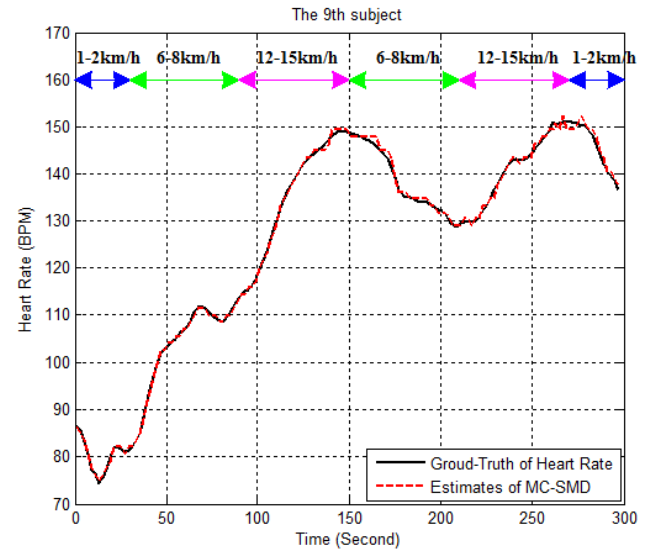
where $\text{BPM}_{\text{true}}(i)$ denotes the ground-truth of heart rate in the i -th time window, $\text{BPM}_{\text{est}}(i)$ denotes the estimated heart rate, and W is the total number of time windows.

A Bland-Altman plot (namely, B-A plot) [35] was the third measurement index. It was used for a combined graphical and statistical interpretation of the two measurement methods. In this analysis, Limit of Agreement (LOA) was calculated, which is defined as $\text{LOA} = [u - 1.96\sigma, u + 1.96\sigma]$, where u is the average difference between each estimate and the associated ground-truth against their average; σ is the standard deviation.

Meanwhile, Pearson correlation was also adopted to reflect the linear correlation between ground-truth values and estimates.

D. RESULTS ANALYSIS

To validate the performance of MC-SMD for heart rate frequency estimation, it was compared with other state-of-the-art techniques that utilize the same datasets. The average absolute error (Error1) and the average absolute error percentage (Error2) for the 12 datasets are listed

**FIGURE 8.** Estimation result for recordings of subject 9.

in Table 2 and Table 3, respectively. We find that MC-SMD had better performance than the other methods. Averaged across the 12 subjects, the absolute estimation error (Error1) of MC-SMD was 1.11 BPM and the error percentage (Error2) was 0.80%. In contrast, TROIKA had a performance of Error1 = 2.42 BPM and Error2 = 1.82%; the Error1 of JOSS was 1.28 BPM and the Error2 was 1.01%; the Error1 of MICROST was 2.58 BPM and the Error2 was 1.99%; the Error1 of SPECTRAP was 1.50 BPM and the Error2 was 1.12%; in [25], Error1 = 1.25 and Error2 = 0.99% (these results were directly adopted from [21]–[25]).

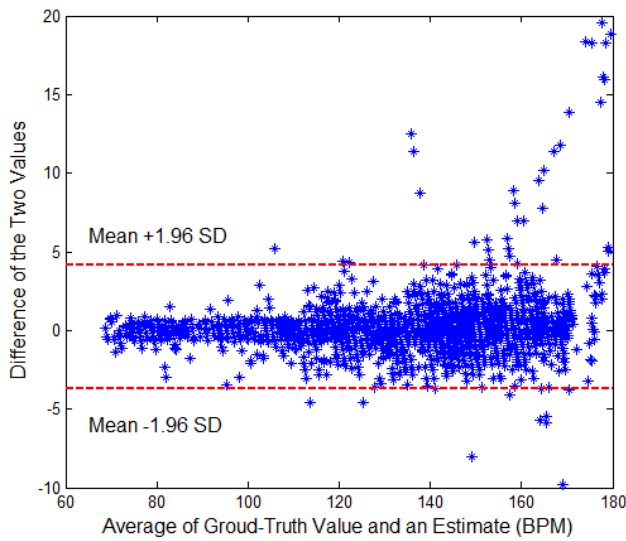


FIGURE 9. The Bland-Altman plot of the estimation results for 12 datasets.

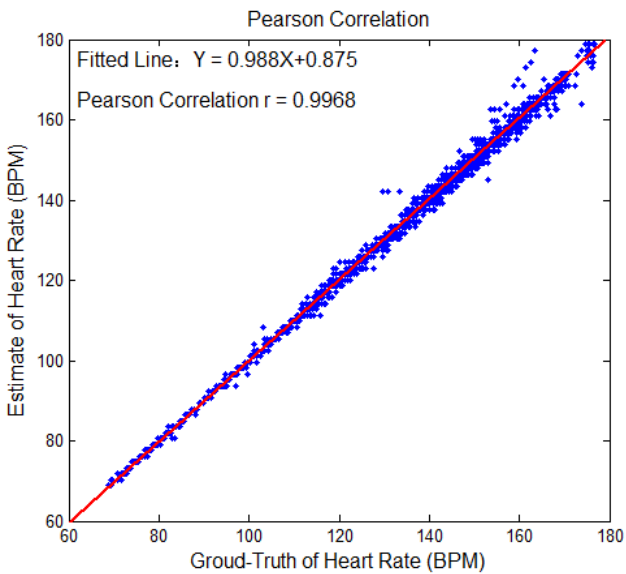


FIGURE 10. Scatter plot of the ground-truth heart rate values versus the associated estimates for the 12 datasets.

To deeply investigate the performance of MC-SMD, Fig. 8 shows the estimated heart rate trace on subject 9 (randomly chosen) as an example. The results show that the estimated heart rate was very close to the ground-truth heart rate. Every small change in the ground truth was estimated with high fidelity.

Moreover, we also evaluated the effectiveness of our algorithm and compared the estimated and the true heart rate. The B-A plot for all 12 datasets is depicted in Fig. 9. The LOA was $[-3.68, 4.13]$ BPM, where $u = 0.2248$, $\sigma = 1.9940$. Fig. 10 gives the scatter plot between the ground-truth heart rate values and the associated estimates. The fitted line was $Y = 0.988X + 0.875$, where X indicates the ground-truth

heart rate values; Y denotes the associated estimates. The Pearson coefficient was 0.9968.

E. DISCUSSIONS

In the experiments the subjects had yellow skin-color and the LED light was green. Skin-color and LED light may affect the MC-SMD's performance. Thus, our further work is to acquire other database at other skin-color and LED light and evaluate the performance of the proposed algorithm.

In addition, MC-SMD works well at low sampling rates, which means low energy consumption in data acquisition and in wireless transmission. Meanwhile, MC-SMD method does not add an extra noise-removal modular, which reduces the complexity of the algorithm. Certainly, we can use a noise-removal modular (such as wavelet denoising, adaptive noise cancellation) in MC-SMD method to improve the robustness.

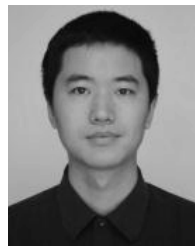
V. CONCLUSION

In this paper, a method named MC-SMD for heart rate estimation using a multi-channel wrist-type PPG during intensive physical activities was presented. The approach consists of two key parts: MC-SMD model and spectral peak tracking method. This new method was tested using datasets of 12 subjects, and ECG was used to validate the derived heart rate. The experimental results indicated that the MC-SMD method has high robustness against strong motion artifacts. Moreover, its performance is better than that of current existing state-of-the-art methods.

REFERENCES

- [1] S. S. Ahrabi, M. Shojafar, H. K. Esfeh, and A. Abraham, "Mathematical modeling of blood flow through an eccentric catheterized artery: A practical approach for a complex system," in *Proc. 14th Int. Conf. Hybrid Intell. Syst.*, Dec. 2014, pp. 315–321.
- [2] S. L. Murphy, J. Xu, and K. D. Kochanek, "Deaths: Final data for 2010," *Nat. Vital Statist. Rep., Centers Disease Control Prevention, Nat. Center Health Statist., Nat. Vital Statist. Syst.*, vol. 61, no. 4, pp. 1–117, 2013.
- [3] J. Allen, "Photoplethysmography and its application in clinical physiological measurement," *Physiol. Meas.*, vol. 28, no. 3, pp. R1–R39, 2007.
- [4] T. Tamura, Y. Maeda, M. Sekine, and M. Yoshida, "Wearable photoplethysmographic sensors—Past and present," *Electronics*, vol. 3, no. 2, pp. 282–302, 2014.
- [5] N. Selvaraj, A. Jaryal, J. Santhosh, K. K. Deepak, and S. Anand, "Assessment of heart rate variability derived from finger-tip photoplethysmography as compared to electrocardiography," *J. Med. Eng. Technol.*, vol. 32, no. 6, pp. 479–484, 2008.
- [6] C. L. Petersen, T. P. Chen, J. M. Ansermino, and G. A. Dumont, "Design and evaluation of a low-cost smartphone pulse oximeter," *Sensors*, vol. 13, no. 12, pp. 16882–16893, 2013.
- [7] J. Lee, W. Jung, I. Kang, Y. Kim, and G. Lee, "Design of filter to reject motion artifact of pulse oximetry," *Comput. Standards Interfaces*, vol. 26, no. 3, pp. 241–249, 2004.
- [8] C. M. Lee and Y. T. Zhang, "Reduction of motion artifacts from photoplethysmographic recordings using a wavelet denoising approach," in *Proc. IEEE-EMBS Asian-Pacific Conf. Biomed. Eng.*, Oct. 2003, pp. 194–195.
- [9] J. Y. A. Foo, "Comparison of wavelet transformation and adaptive filtering in restoring artefact-induced time-related measurement," *Biomed. Signal Process. Control*, vol. 1, no. 1, pp. 93–98, 2006.
- [10] M. Raghuram, K. V. Madhav, E. H. Krishna, and K. A. Reddy, "Evaluation of wavelets for reduction of motion artifacts in photoplethysmographic signals," in *Proc. 10th ISSPA*, May 2010, pp. 460–463.

- [11] X. Sun, P. Yang, Y. Li, Z. Gao, and Y.-T. Zhang, "Robust heart beat detection from photoplethysmography interlaced with motion artifacts based on empirical mode decomposition," in *Proc. IEEE-EMBS*, Jan. 2012, pp. 775–778.
- [12] Y. Zhang, B. Liu, and Z. Zhang, "Combining ensemble empirical mode decomposition with spectrum subtraction technique for heart rate monitoring using wrist-type photoplethysmography," *Biomed. Signal Process. Control*, vol. 21, pp. 119–125, Aug. 2015.
- [13] S. Seyedtabaii and L. Seyedtabaii, "Kalman filter based adaptive reduction of motion artifact from photoplethysmographic signal," *World Acad. Sci., Eng. Technol.*, vol. 37, pp. 173–176, Feb. 2008.
- [14] Y.-S. Yan, C. C. Y. Poon, and Y.-T. Zhang, "Reduction of motion artifact in pulse oximetry by smoothed pseudo Wigner-Ville distribution," *J. Neuroeng. Rehabil.*, vol. 2, no. 1, pp. 1–9, 2005.
- [15] M. J. Hayes and P. R. Smith, "Artifact reduction in photoplethysmography," *Appl. Opt.*, vol. 37, no. 31, pp. 7437–7446, 1998.
- [16] H. Fukushima, H. Kawanaka, M. S. Bhuiyan, and K. Oguri, "Estimating heart rate using wrist-type photoplethysmography and acceleration sensor while running," in *Proc. IEEE-EMBC*, Aug./Sep. 2012, pp. 2901–2904.
- [17] B. S. Kim and S. K. Yoo, "Motion artifact reduction in photoplethysmography using independent component analysis," *IEEE Trans. Biomed. Eng.*, vol. 53, no. 3, pp. 566–568, Mar. 2006.
- [18] M.-Z. Poh, N. C. Swenson, and R. W. Picard, "Motion-tolerant magnetic earring sensor and wireless earpiece for wearable photoplethysmography," *IEEE Trans. Inf. Technol. Biomed.*, vol. 14, no. 3, pp. 786–794, May 2010.
- [19] R. Yousefi, M. Nourani, S. Ostadabbas, and I. Panahi, "A motion-tolerant adaptive algorithm for wearable photoplethysmographic biosensors," *IEEE J. Biomed. Health Informat.*, vol. 18, no. 2, pp. 670–681, Mar. 2014.
- [20] Z. Zhang, "Heart rate monitoring from wrist-type photoplethysmographic (PPG) signals during intensive physical exercise," in *Proc. GlobalSIP*, Dec. 2014, pp. 698–702.
- [21] Z. Zhang, Z. Pi, and B. Liu, "TROIKA: A general framework for heart rate monitoring using wrist-type photoplethysmographic signals during intensive physical exercise," *IEEE Trans. Biomed. Eng.*, vol. 62, no. 2, pp. 522–531, Feb. 2015.
- [22] Z. Zhang, "Photoplethysmography-based heart rate monitoring in physical activities via joint sparse spectrum reconstruction," *IEEE Trans. Biomed. Eng.*, vol. 62, no. 8, pp. 1902–1910, Aug. 2015.
- [23] S. Zhu, K. Tan, X. Zhang, Z. Liu, and B. Liu, "MICROST: A mixed approach for heart rate monitoring during intensive physical exercise using wrist-type PPG signals," in *Proc. 37th IEEE-EMBC*, Aug. 2015, pp. 2347–2350.
- [24] B. Sun and Z. Zhang, "Photoplethysmography-based heart rate monitoring using asymmetric least squares spectrum subtraction and Bayesian decision theory," *IEEE Sensors J.*, vol. 15, no. 12, pp. 7161–7168, Dec. 2015.
- [25] M. B. Mashhadi, E. Asadi, M. Eskandari, S. Kiani, and F. Marvasti, "Heart rate tracking using wrist-type photoplethysmographic (PPG) signals during physical exercise with simultaneous accelerometry," *IEEE Signal Process. Lett.*, vol. 23, no. 2, pp. 227–231, Feb. 2016.
- [26] S. F. Cotter, B. D. Rao, K. Engan, and K. Kreutz-Delgado, "Sparse solutions to linear inverse problems with multiple measurement vectors," *IEEE Trans. Signal Process.*, vol. 53, no. 7, pp. 2477–2488, Jul. 2005.
- [27] Y. Mendelson and B. D. Ochs, "Noninvasive pulse oximetry utilizing skin reflectance photoplethysmography," *IEEE Trans. Biomed. Eng.*, vol. 35, no. 10, pp. 798–805, Oct. 1988.
- [28] P. Gong, J. Ye, and C. Zhang, "Robust multi-task feature learning," in *Proc. 18th ACM SIGKDD*, 2012, pp. 895–903.
- [29] (Sep. 2007). *CORE Discussion Paper, 2007/76*, accessed on Jun. 25, 2016. [Online]. Available: http://www.optimization-online.org/DB_FILE/2007/09/1784.pdf
- [30] X. Chen, W. Pan, J. T. Kwok, and J. G. Carbonell, "Accelerated gradient method for multi-task sparse learning problem," in *Proc. 9th ICDM*, Dec. 2009, pp. 746–751.
- [31] T. Zhang, S. Liu, N. Ahuja, M.-H. Yang, and B. Ghanem, "Robust visual tracking via consistent low-rank sparse learning," *Int. J. Comput. Vis.*, vol. 111, no. 2, pp. 171–190, 2014.
- [32] J. Liu, S. Ji, and J. Ye, "Multi-task feature learning via efficient $L_{2,1}$ -norm minimization," in *Proc. 25th Artif. Intell.*, 2009, pp. 339–348.
- [33] P. H. C. Eilers, "A perfect smoother," *Anal. Chem.*, vol. 75, no. 14, pp. 3631–3636, 2003.
- [34] Z. Zhang, "Undergraduate student compete in the IEEE signal process cup: Part 3," *IEEE Signal Process. Mag.*, vol. 32, no. 6, pp. 113–116, Nov. 2015.
- [35] J. M. Bland and D. G. Altman, "Statistical methods for assessing agreement between two methods of clinical measurement," *Lancet*, vol. 327, no. 8476, pp. 307–310, Feb. 1986.



JIIPPING XIONG (S'08–M'06) received the B.S. degree in electronics and communication engineering and the Ph.D. degree in communication and information system from the University of Science and Technology of China in 2001 and 2006. He was a Visiting Scholar with the Department of Computer Science and Engineering, University of Minnesota, Minneapolis, MN, USA, from 2012 to 2013. Currently, he is an Associate Professor of Computer Engineering with Zhejiang Normal University, China.

His research interests include compressive sensing, computer vision, networking, information security, and signal processing.



LISANG CAI (S'14) received the B.S. degree in applied physics from the Huzhou Teachers College of China in 2014. She is currently pursuing the degree in physical electronics with Zhejiang Normal University, China.

Her research interests include compressive sensing, information security, machine learning, and signal processing.



DINGDE JIANG (S'08–M'09) received the Ph.D. degree in communication and information systems from the University of Electronic Science and Technology of China, Chengdu, China, in 2009. He is a Professor with the College of Information Science and Engineering, Northeastern University, Shenyang, China. From 2013 to 2014, he was a Visiting Scholar with the Department of Computer Science and Engineering, University of Minnesota, Minneapolis, MN, USA. His research focuses on network measurement, modeling and optimization, performance analysis, network management, and network security in communication networks, particularly in software-defined networks, information-centric networking, energy-efficient networks, and cognitive networks.

He currently serves as an Editor for one international journal. He has served as a Technical Program Committee Member for several international conferences. He has received the best paper award at international conferences.



Houbing Song (M'12–SM'14) received the Ph.D. degree in electrical engineering from the University of Virginia, Charlottesville, VA, in 2012.

In 2012, he joined the Department of Electrical and Computer Engineering, West Virginia University Institute of Technology, Montgomery, WV, where he is currently an Assistant Professor and the Founding Director of both the Security and Optimization for Networked Globe Laboratory, and West Virginia Center of Excellence for Cyber-Physical Systems sponsored by the West Virginia Higher Education Policy Commission. In 2007, he was an Engineering Research Associate with the Texas A&M Transportation Institute. He is the editor of six books, including *Smart Cities: Foundations and Principles* (Hoboken, NJ, USA: Wiley, 2016), *Cyber-Physical Systems: Foundations, Principles and Applications* (Waltham, MA, USA: Elsevier, 2016), and *Industrial Internet of Things: Cybermanufacturing Systems* (Cham, Switzerland: Springer, 2016). He has published more than 100 academic papers in peer-reviewed international journals and conferences. His research interests lie in the areas of cyber-physical systems, Internet of Things, cloud computing, big data, connected vehicle, wireless communications and networking, and optical communications and networking.

Dr. Song is a member of ACM. He was the first recipient of the Golden Bear Scholar Award, the highest faculty research award at WVU Tech. He is an Associate Editor for several international journals, including the IEEE ACCESS and the *KSII Transactions on Internet and Information Systems*, and a Guest Editor of more than ten special issues. He was the General Chair of several international workshops, including the first IEEE International Workshop on Security and Privacy for Internet of Things and Cyber-Physical Systems within the IEEE ICC, 2015, in London, U.K., and the first IEEE International Workshop on Big Data Analytics for Smart and Connected Health within the IEEE CHASE, held 2016, in Washington, DC. He also served as the Technical Program Committee Chair of the fourth IEEE International Workshop on Cloud Computing Systems, Networks, and Applications (CCSNA), held 2015, in San Diego, USA. He is serving as the Publicity Chair of the 2017 IEEE Wireless Communications and Networking Conference (WCNC) to be held 2017, in San Francisco, CA, and the Technical Program Committee Chair of the fifth IEEE International Workshop on CCSNA to be held 2016, in Washington, DC. He has served on the Technical Program Committee for numerous international conferences, including ICC, GLOBECOM, INFOCOM, and WCNC.



XIAOWEI HE (S'92–M'02) was born in China in 1968. He received the B.S. degree in mathematics from Zhejiang Normal University in 1992 and the M.S. degree in computer application from Zhejiang University, Jinhua, China, in 2000. He is currently an Associate Professor and also a Master Tutor of the Computer Software and Theory with Zhejiang Normal University. His research interests include image processing, signal processing, and inverse problems.

• • •